Continental Shelf Research 96 (2015) 27–33

Contents lists available at ScienceDirect

Continental Shelf Research

journal homepage: www.elsevier.com/locate/csr

Research papers

Trace metal behavior along fluvio-marine gradients in the Samborombón Bay, outer Río de la Plata estuary, Argentina

L.M. Tatone [a,b,*], C. Bilos [a], C.N. Skorupka [a], J.C. Colombo [a,c]

[a] Laboratorio de Química Ambiental y Biogeoquímica, Facultad de Ciencias Naturales y Museo, Universidad Nacional de La Plata, Av. Calchaqui km 23500, 1888 Florencio Varela, Buenos Aires, Argentina
[b] Consejo Nacional de Investigaciones Científicas y Técnicas (CONICET), Av. Rivadavia 1917, CP C1033AA Ciudad de Buenos Aires, Argentina
[c] Comisión de Investigaciones Científicas (CIC), Provincia de Buenos Aires, Calle 10 y 526, 1900 La Plata, Argentina

ARTICLE INFO

Article history:
Received 27 May 2014
Received in revised form
15 January 2015
Accepted 20 January 2015
Available online 22 January 2015

Keywords:
Heavy metals
Sediments
Turbidity maximum zone
Samborombón Bay
Río de la Plata

ABSTRACT

Water and sediment samples were collected in the Samborombón Bay, outer Río de la Plata estuary to evaluate the dynamics of trace metals along the fluvial–marine transition. This estuarine environment presented strong salinity (0.11–31.4) and turbidity (21 to >999 mg L^{-1}) gradients with a consistent turbidity maximum zone (TMZ: >1 g suspended solids L^{-1}) in the low salinity region. Suspended particulate metals showed different spatial patterns: homogeneous distributions (Fe, Zn) and progressive enrichment from the TMZ to the maritime area (Cu, Ni). The influence of the TMZ is clearly reflected by the enrichment of flocculated clays which in turns control the distribution of sedimentary TOC and trace metals resulting in a prevailing decreasing land–sea gradient. Mn has a particular behavior along the salinity gradient denoting intense dissolved-particulated phase changes both in the water column and bottom sediments. An average 36% drop of particulate Mn observed in parallel with a strong dissolved peak suggests a rapid Mn desorption/dissolution in the water column whereas bottom sediments display an average 72% Mn enrichment in the TMZ relative to the riverine sector reflecting the diffusive escape from anoxic sediments and reprecipitation in oxic surface layers.

© 2015 Elsevier Ltd. All rights reserved.

1. Introduction

Estuaries form complex and variable linkages between fluvial and marine environments acting as effective sediment traps (Biggs and Howell, 1984; Woodruff et al., 2001), and typically developing a turbidity maximum zone (TMZ) with highest suspended solid concentrations at the beginning of the saline intrusion (Morris et al., 1982; Wu et al., 2012). Dissolve-particulate phase changes and prevailing adsorption onto heterogeneously distributed solids peaking at the TMZ strongly condition the overall dynamics and fate of trace metals in estuarine environments (Hughes et al., 1998).

The Río de la Plata located on the eastern coast of South America is the most prominent estuarine environment in Argentina (Fig. 1). It is a funnel-shaped, turbid, shallow coastal plain estuary with a total surface area of 35,000 km^2 and a huge particulate load of 90 million t of solids per year (Framiñan et al., 1999). It is formed by the confluence of two major South American rivers, the Paraná and Uruguay, with mean discharges of 16,000 and 6000 m^3 s^{-1} respectively. A submerged shoal divides the estuary into an inner and an outer system; the inner sector is a very shallow (1–5 m) fluvial area severely affected by crude effluent discharges containing persistent organic pollutants (POPs), hydrocarbons and trace metals (Colombo et al., 2005a,b, 2006; Tatone et al., 2009, 2013) from the densely populated and industrialized Metropolitan Buenos Aires. The outer region is a 22,000 km^2 mixohaline system, with depths of 5–25 m and vertical stratification, sparsely populated and mostly devoted to agriculture. Most of the solid load of the estuary comes from the Bermejo river which drains rainy Andean food plains and discharges its highly turbid waters (~6000 mg l^{-1}) into the Paraná river, 1300 km north from Buenos Aires (Drago and Amsler, 1988, 1998; Depetris et al. 2003; Moreira et al., 2013). This load transported by the Paraná river forms a distinct water corridor along the Argentinean coast of the Río de la Plata (Piedra-Cueva and Fossati, 2007). Associated to the bottom topography, at the tip of the salt wedge, the flocculation of suspended clays and the tidal resuspension produce a turbidity front (Framiñan and Brown, 1996; Guerrero et al., 1997; Acha et al., 2008). The extension and

* Corresponding author at: Laboratorio de Química Ambiental y Biogeoquímica, Av. Calchaqui km 23500, 1888 Florencio Varela, Buenos Aires, Argentina. Fax: +54 11 4275 8266.
E-mail address: leatatone@yahoo.com.ar (L.M. Tatone).

http://dx.doi.org/10.1016/j.csr.2015.01.007
0278-4343/© 2015 Elsevier Ltd. All rights reserved.

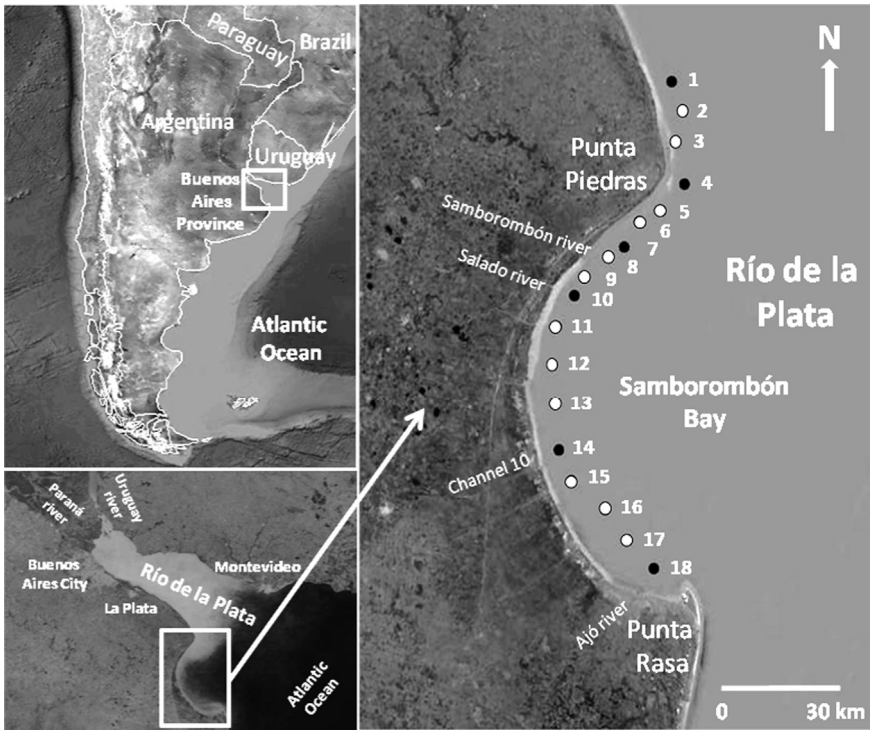

Fig. 1. Study area and location of sampling sites in the Río de la Plata estuary (black dots indicate transects at 1, 3 and 6 km offshore).

location of the TMZ is determined by the tides, winds, and fluctuating river discharges which control water density and circulation (Framiñan and Brown, 1996). Most of the turbidity flux is directed to the southwest to the Samborombón Bay which is an extensive, very shallow, mixohaline depositional environment delimited by Punta Piedras (upstream) and Punta Rasa which constitutes the outer maritime limit of the estuary (Fig. 1). In addition to the Paraná discharge, the bay receives the contribution of several rivers and channels that drain the Pampean plain (Salado, Samborombón and Ajó rivers, channels 15, 10, A and 1; Carol et al., 2014). The Samborombón Bay is a RAMSAR site since 1997 and has been described as an important nursery ground for important commercial fish (Lasta, 1995; Mianzan et al., 2001).

In this paper we evaluate the behavior and distribution of trace metals along fluvio-marine gradients through the turbidity maximum zone in the Samborombón Bay, outer Río de la Plata estuary.

2. Materials and methods

2.1. Sampling

Samples were collected in 2007–2008 covering 140 km in the outer Río de la Plata estuary (Fig. 1). Water temperature (°C), depth (m), dissolved oxygen (mg L^{-1}), conductivity (mS cm^{-1}), and turbidity (mg L^{-1}) were measured in situ using a multi-parameter probe (TOA Water Quality Checker WQC 20-A). Conductivity values were transformed into salinity and expressed in Practical Salinity Units (PSU). Surface water samples ($n=12$) were collected manually using 1-L amber glass bottles at 1 and 6 km from the shore along the transects. Surface sediments ($n=30$) were collected 6 km offshore at 18 stations and at 1, 3 and 6 km from the coast along the 6 transects (Fig. 1) with a "Van Veen" style Hydro-Bios stainless steel grab sampler. Each sediment sample was carefully taken from the central portion of the dredge with a plastic spatula and stored in pre-cleaned glass jars.

2.2. Chemical analyses

Water samples were vacuum filtered through 0.45 μm (45 mm diameter) cellulose acetate filters to separate suspended particulate matter (SPM). Sediment samples were homogenized and splitted for the determination of the grain size composition (sieve and pipet method; Folk, 1980), total organic carbon (TOC) and nitrogen (TN) contents (catalytic combustion with a Thermo Finnnigan, CE FlashEA 1112 elemental analyzer) and the determination of trace metals. Filters with SPM and about 1.0 g of homogenized sediment were digested with aqua regia (3:1 v/v, HCl to HNO_3) and H_2O_2 at 100 °C (Hseu et al., 2002). The extracts were centrifuged, diluted to 25 ml with deionized water and stored in polyethylene bottles. All plastic material and glassware was thoroughly washed with acid (10% HNO_3) and rinsed with deionized water.

Metal concentrations were determined using a Thermo Elemental Solaar M5 atomic absorption spectrophotometer equipped with a deuterium background corrector. SPM and sediment samples were measured in an air-acetylene flame while dissolved Mn concentrations were measured by using a GF95 graphite furnace with autosampler. Procedural blanks were negligible. The precision of trace metal determinations as the relative standard deviation (RSD) tested through the analysis of 5 duplicate samples was below 10%. The method recovery was tested through triplicate analysis of Certified Reference Soil (CRM020-050 RTC). The average recoveries for each metal ranged from 72% to 110% (Fe = 106.4 ± 13.7%; Mn = 97.3 ± 5.3%; Cu = 99.7 ± 2.8%; Zn = 109.6 ± 5.9%; Cr = 104.1 ± 11.8; Pb = 109.4 ± 3.4% and Ni = 72.4 ± 6.6%; Table 1). The accuracy of TOC and TN determinations, evaluated through the analysis of certified reference materials including a high organic content sediment (B2150 Elemental MicroAnalysis Ltd.; %C = 6.10 and %N = 0.46) and a low organic content soil (B2152 Elemental MicroAnalysis Ltd.; %C = 1.52 and %N = 0.13) ranged from 85% to 115%.

Table 1
Average recovery of triplicate analysis for certified reference material (CRM020-050 RTC).

Metal	Certified values ($\mu g\ g^{-1}$)	Analytical values ($\mu g\ g^{-1}$)	Recovery (%)
Fe	191706 ± 17737	203897 ± 26349	106 ± 13.7
Mn	945 ± 92.8	920 ± 50.55	97.3 ± 5.35
Cu	729 ± 69.9	726 ± 20.14	100 ± 2.76
Zn	3011 ± 287	3301 ± 177	110 ± 5.89
Cr	13.6 ± 5.65	14.2 ± 1.60	104 ± 11.8
Pb	5111 ± 692	5592 ± 173	109 ± 3.38
Ni	16.9 ± 5.42	12.2 ± 1.11	72.4 ± 6.57

3. Results and discussion

3.1. Water quality parameters

The survey was carried out in 0.5–6.3 m water depths, with temperature ranging from 18.8 to 21.6 °C and dissolved oxygen between 8.0 and 13.9 mg L^{-1} indicating relatively well oxygenated waters. As expected for an estuarine environment, salinity show > 2 orders magnitude variability (0.11–31.4) reflecting the gradient from fresh (< 0.5) to polihaline water (18–30) with only one value in the euhaline domain (> 30). Turbidity also displays large variability (21 to > 999 mg L^{-1}) with a general decreasing seaward trend and also with distance offshore. Laboratory SPM determinations confirmed "in situ" turbidity measurements and displayed a highly significant correlation (R^2 = 0.99; slope = 1.3).

Salinity and turbidity presented clear spatial gradients which allow the discrimination of three zones within the Bay (Fig. 2): a freshwater zone with low salinity (0.11–0.22) and moderate turbidity (210–340 mg L^{-1}), the turbidity maximum zone (TMZ) where the flocculation of clays due to the increasing ionic gradient (salinity: 0.16–9.37) produce a significant increase in turbidity (450 to > 999 mg L^{-1}), and a marine, more eutrophic zone (greener waters) with higher salinity (12.3–31.4) and lower turbidity (21–66 mg L^{-1}). Phytoplankton dynamics is effectively controlled by turbidity in the upper river (light-limitation) but immediately downstream the turbidity front, water clarification and abundant nutrient availability results in a sharp rise of pigments (Carreto et al., 2008). Superimposed on this general estuarine gradient, the direct discharge of rivers and channels into Samborombón Bay (Salado, Ajó and Channel 10) produce secondary offshore gradients with decreasing salinity and increasing turbidity close to the embouchures (Fig. 2).

3.2. Suspended particulate matter (SPM)

Table 2 presents total SPM concentrations, TOC, C/N and trace metal contents of the suspended material. SPM ranges from 7.4 to 1291 mg L^{-1} along the land–sea gradient following the turbidity patterns described above. As salinity increases, SPM progressively decrease after the TMZ maxima (Fig. 3a). In contrast, the TOC contents of SPM (2.3 ± 0.9%) show a positive correlation with salinity (R^2 = 0.50) increasing in the maritime zone while C/N ratios (8.6 ± 1.2) generally decrease (9.6–6.5) reflecting stronger influence of marine planktonic over terrestrial inputs (Hedges et al., 1997). Two samples affected by the Ajó river discharge disrupt the decreasing C/N ratio trend in the high salinity area (Fig. 3a), reflecting the influence of local river discharges along the general terrestrial–planktonic estuarine gradient.

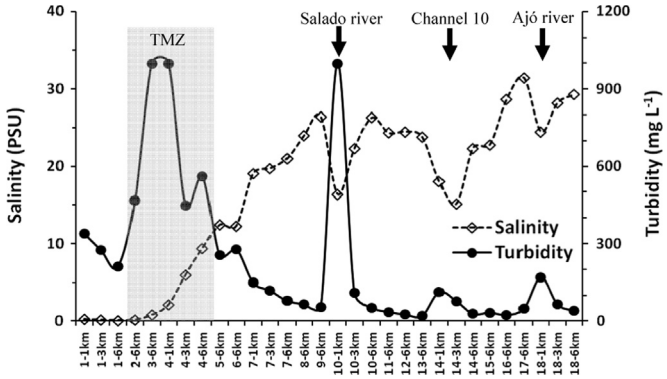

Fig. 2. Variation of salinity and turbidity along the Samborombón Bay. Turbidity maximum zone (TMZ: shaded area) and principal affluents (black arrows) are indicated.

SPM trace metal concentrations show distinctive patterns: Fe and Zn are relative homogeneous (48223 ± 5111 $\mu g\ g^{-1}$, RSD: ± 11%; 108 ± 16.3 $\mu g\ g^{-1}$, RSD: ± 15%, respectively), Cr was only detected in freshwaters and the TMZ (34.5 ± 6.4 $\mu g\ g^{-1}$, RSD: ± 18%) whereas Pb was below the detection limit in all stations. Cu and Ni show large variability (87.1 ± 84.1 $\mu g\ g^{-1}$, RSD: ± 97% and 75.7 ± 68.9 $\mu g\ g^{-1}$, RSD: ± 91%, respectively) and a decreasing trend with SPM abundance (R^2_{Cu} = 0.83; R^2_{Ni} = 0.92; Fig. 3b). This pattern reflects the transition from the terrestrial upper zone of the Bay dominated by the solid inputs from the Paraná river with lower trace metal contents to the maritime area, where trace metals result enriched in the more organic and scarce SPM. In contrast, Zn presents relatively homogeneous concentrations increasing with SPM abundance (R^2 = 0.39; Fig. 3b). Mn displays a particular behavior with a sharp drop at the TMZ reflecting intense dissolved–particulated phase remobilization (see Section 3.4).

3.3. Bottom sediments

Table 3 presents the TOC contents, C/N and trace metal concentrations in sediments and the correlation matrix among the different parameters is shown in Table 4. Sediments were predominately silty-clays (clay: 60 ± 20%; silt: 29 ± 12%) with low sand contents (11 ± 22%), excepted in the marine zone of the bay which is significantly enriched in sands (14–1 km, 16–6 km, 17–6 km, 18–1 km and 18–3 km: 25–78%; Fig. 4). This grain size composition reflects the influence of the TMZ increasing the clay contents of the bottom i.e. flocculation, and the presence of sand shoals in the maritime zone. Sediment TOC ranges between 0.2% and 1.5% (1.1 ± 0.3%) similar to values reported for the most industrialized region of the estuary (Tatone et al., 2009) and about half of suspended particle TOC contents. Sedimentary TOC show a positive covariation with clays (r = 0.84) and negative with sands (r = −0.87; Table 4) with no apparent spatial trends. In contrast to the seaward-decreasing trend of SPM C/N, sediment C/N ratios are very uniform (8.3–9.4 or 8.8 ± 0.3) and do not show any consistent spatial pattern. The significantly lower TOC contents and more homogeneous C/N ratios of bottom sediments relative to SPM reflect the rapid decay of the marine component and preferential preservation of the terrestrial signal during early digenesis of organic matter and sediment burial.

The average trace metal concentration in surface sediments follow their natural abundance in the earth crust decreasing from Fe (33479 ± 7971 $\mu g\ g^{-1}$) > Mn (587 ± 202 $\mu g\ g^{-1}$) > Zn (81 ± 22 $\mu g\ g^{-1}$) > Cu (23 ± 7.3 $\mu g\ g^{-1}$) ~ Cr (21 ± 7.4 $\mu g\ g^{-1}$) > Pb (15 ± 4.8 $\mu g\ g^{-1}$) ~ Ni (15 ± 5.1 $\mu g\ g^{-1}$). These concentrations are lower than those reported for the most industrialized upper part of the estuary especially for Pb, Zn and Cr (~2 times lower; Tatone et al., 2009). In contrast to this impacted area which presented exponentially-decreasing trace metal offshore gradients, no offshore patterns are observed in the Samborombón Bay indicating the virtual absence of point coastal pollution sources.

The ecotoxicological status of the Bay concerning trace metals was evaluated through the comparison with Canadian sediment quality guidelines (CCME, 2001), considering the Sediment Quality

Table 2
SPM concentrations, TOC, C/N and trace metals in suspended material.

Stations	SPM	TOC	C/N	Fe	Mn	Zn	Cu	Ni	Cr	Pb
	(mg L^{-1})	(%)		(μg g^{-1})						
1–1 km	323	1.74	9.65	50913	1273	115.3	38.1	30.7	37.0	N.D.
1–6 km	187	1.60	9.59	49163	1320	129.6	48.4	49.3	45.5	N.D.
3–6 km	1291	1.28	8.88	50086	605	116.7	39.4	26.5	35.5	N.D.
4–1 km	1259	1.33	8.87	47262	842	111.0	37.0	24.3	32.7	N.D.
4–6 km	669	1.47	9.14	50418	1026	127.8	43.2	29.8	36.0	N.D.
7–1 km	123	2.71	7.73	44434	874	112.3	48.7	38.1	29.9	N.D.
7–6 km	54.5	2.35	6.55	42523	763	114.1	68.6	75.9	N.D.	N.D.
10–6 km	19.5	2.40	6.86	52728	901	108.4	124.4	109.3	N.D.	N.D.
14–1 km	82.5	4.21	7.53	38423	957	101.2	65.7	63.9	N.D.	N.D.
14–6 km	7.4	3.13	N.D.	58266	1209	68.2	322.0	243.2	N.D.	N.D.
18–1 km	173	2.27	9.41	45805	1135	93.1	43.0	40.2	25.1	N.D.
18–6 km	16.1	3.22	10.3	48651	1130	103.8	167.4	177.4	N.D.	N.D.
Mean	**350**	**2.31**	**8.59**	**48223**	**1003**	**108.5**	**87.1**	**75.7**	**34.5**	
SD	469	0.89	1.24	5111	218	16.3	84.1	68.9	6.4	

N.D.=not detected.

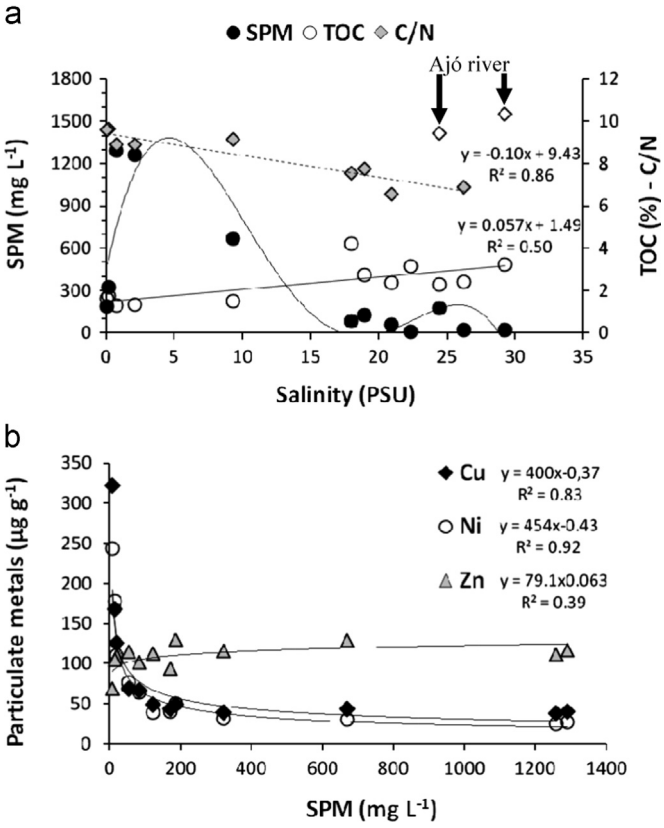

Fig. 3. Variation of **s**uspended particulate matter (SPM), TOC and C/N ratios along salinity gradients (**a**) and of particulate Cu, Ni and Zn concentrations vs. SPM (**b**).

Guideline (SQG) and the Probable Effect Level (PEL) which define three ranges of chemical concentrations associated to increasing adverse biological effects (rare: < SQG; occasional: > SQG and < PEL; frequent: > PEL). In contrast to coastal stations from the upper estuary where Cr, Zn, Cu and Pb normally exceeded the SQG values (Tatone et al., 2009), the concentrations of most trace elements are lower than the SQG for freshwater (35–123 μg g^{-1}) and marine sediments (18.7–124 μg g^{-1}). In the case of Cu, the concentrations are lower than the SQG for freshwater sediments (35.7 μg g^{-1}), but some samples are in the range between the SQG and PEL for marine sediments (18.7–108 μg g^{-1}) suggesting the possibility of very occasional adverse biological effects for aquatic biota in this area.

Table 3
TOC contents, C/N and trace metal concentrations in sediments.

Stations	TOC	C/N	Fe	Mn	Zn	Cu	Cr	Pb	Ni
	(%)		(μg g^{-1})						
1–1 km	1.0	8.8	37190	598	90.0	24.6	23.0	17.4	16.5
1–3 km	1.2	8.5	37979	652	98.4	27.6	26.8	19.7	18.5
1–6 km	1.0	8.6	32234	506	81.7	22.2	20.7	16.1	14.7
2–6 km	1.3	8.8	39759	956	99.0	28.8	28.3	20.7	18.6
3–6 km	1.3	8.7	34688	910	87.5	25.2	24.7	18.7	16.5
4–1 km	1.5	8.4	41950	1008	102.6	28.6	27.3	20.0	19.5
4–3 km	1.3	8.7	40157	626	96.0	27.7	24.6	18.7	19.0
4–6 km	1.4	8.6	37680	923	93.0	27.9	26.2	19.7	18.8
5–6 km	1.1	8.5	46933	472	119.2	35.0	35.8	24.9	21.6
6–6 km	1.5	8.5	34044	1052	84.2	25.5	23.4	18.0	17.3
7–1 km	1.3	8.3	41067	488	90.0	29.1	26.6	16.4	19.9
7–3 km	1.2	9.0	37362	448	91.7	28.3	27.3	18.2	18.3
7–6 km	1.1	9.0	39979	404	97.2	30.0	28.4	18.6	20.2
8–6 km	1.3	8.9	43152	479	109.1	33.6	29.8	21.2	22.3
9–6 km	1.2	8.4	37457	409	91.8	27.5	25.7	16.9	18.1
10–1 km	1.1	8.6	33126	735	78.5	22.6	19.0	14.6	14.4
10–3 km	1.0	–	32295	547	76.6	21.7	20.5	14.8	13.8
10–6 km	1.2	–	37324	627	96.8	31.0	27.3	19.7	19.3
11–6 km	1.2	9.2	35309	476	85.2	25.7	22.3	14.9	16.3
12–6 km	1.4	8.9	35676	688	85.6	25.7	22.8	15.7	16.7
13–6 km	1.3	8.9	30892	445	75.7	22.1	18.3	13.0	13.1
14–1 km	0.7	9.2	24366	524	52.6	12.9	10.9	9.5	7.7
14–3 km	1.2	8.8	32079	472	76.1	21.3	17.1	12.1	13.0
14–6 km	1.0	9.0	28460	449	66.3	18.8	14.9	10.5	11.7
15–6 km	1.4	8.7	35129	602	83.8	22.6	18.6	13.2	15.2
16–6 km	0.7	9.3	21883	323	48.4	12.3	10.4	8.2	8.1
17–6 km	0.2	–	17627	276	33.9	6.5	7.5	7.3	4.0
18–1 km	0.4	–	12013	424	27.3	7.6	4.6	5.3	3.7
18–3 km	0.6	–	19539	616	44.1	11.0	9.2	8.3	6.4
18–6 km	0.8	9.4	27032	484	62.3	15.7	14.3	9.8	10.1
Mean	**1.1**	**8.8**	**33479**	**587**	**80.8**	**23.3**	**21.2**	**15.4**	**15.1**
SD	0.3	0.3	7971	202	22	7.3	7.4	4.8	5.1

With the exception of Mn, metals showed a strong significant correlation among them (r=0.94–0.99), with clays (r=0.75–0.88) and with the TOC content of sediments (r=0.75-0.85; Table 4), reflecting the control of grain size over TOC and trace metal distributions (Zhang et al., 2009). Accordingly, there is an apparent seaward decreasing trend of sedimentary metals from the TMZ to the marine sector following the decrease of clay contents.

In order to comparatively evaluate the behavior of trace metals in SPM and sediments, Fig. 5 presents their concentrations against TOC contents for both matrices. Trace metals concentrations are generally lower in sediments relative to SPM reflecting their close association with finer particles (Stecko and Bendell-Young, 2000),

Table 4
Pearson's correlation coefficients for metal concentrations, TOC and grain size composition of sediments (significant values at $p < 0.05$ are indicated in bold).

	Fe	Mn	Zn	Cu	Cr	Pb	Ni	TOC	Sand	Silt	Clay
Fe	1										
Mn	0.35	1									
Zn	**0.99**	**0.38**	1								
Cu	**0.97**	0.36	**0.98**	1							
Cr	**0.97**	**0.37**	**0.98**	**0.98**	1						
Pb	**0.94**	**0.47**	**0.96**	**0.95**	**0.98**	1					
Ni	**0.98**	**0.38**	**0.98**	**0.99**	**0.98**	**0.95**	1				
TOC	**0.83**	**0.59**	**0.83**	**0.84**	**0.77**	**0.75**	**0.85**	1			
Sand	**−0.85**	−0.36	**−0.85**	**−0.83**	**−0.79**	**−0.74**	**−0.84**	**−0.87**	1		
Silt	0.10	0.23	0.11	0.03	0.01	0.07	0.06	0.15	**−0.39**	1	
Clay	**0.85**	0.25	**0.84**	**0.88**	**0.84**	**0.75**	**0.86**	**0.84**	**−0.84**	−0.17	1

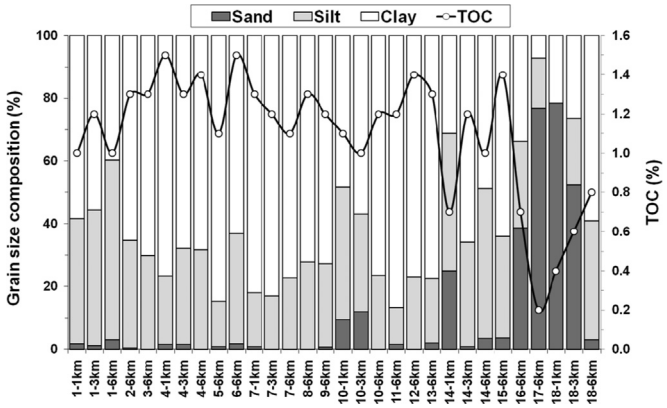

Fig. 4. Grain size composition and TOC content of surficial sediments.

but at the TMZ the concentrations are more alike (darker points in Fig. 5) probably reflecting the bottom enrichment in finer particles flocculated in this area (see Fig. 4). Trace metals display different patterns against TOC: Fe, Mn and Zn appear to level-off whereas Cu and Ni show an exponential increase indicating enrichment in marine SPM. The particular trace metal dynamics of Mn in the TMZ is also evidenced by the inverted SPM < sediment concentration trend in this area (see Section 3.4).

3.4. Mn behavior in the TMZ

Mn displays a particular behavior along the salinity gradient denoting intense dissolved–particulated phase changes both in the water column and bottom sediments. Suspended particles show the highest Mn concentrations in the riverine sector followed by a sharp drop at the TMZ (1297 ± 33 to $825 \pm 211\ \mu g\ g^{-1}$) and a

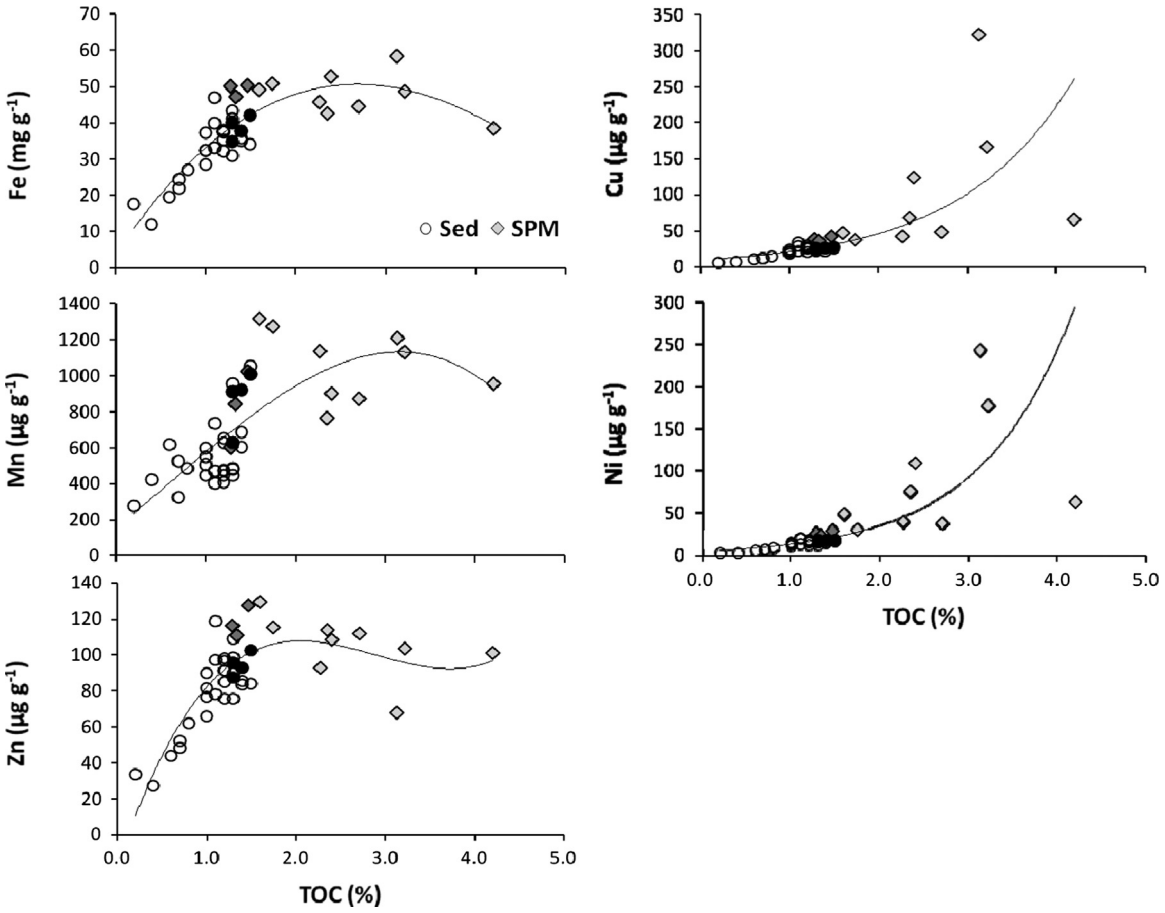

Fig. 5. Variation of trace metal concentrations in surface sediments and SPM vs. TOC contents (samples from the turbidity maximum zone are indicated by darker points).

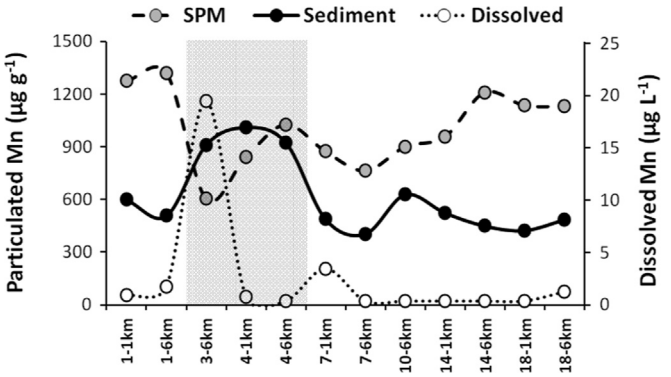

Fig. 6. Mn concentrations in the turbidity maximum zone (shaded area). Values of dissolved Mn smaller than the detection limit were taken as the half of detection limit.

progressive increase in the maritime area ($996 \pm 164\ \mu g\ g^{-1}$; Fig. 6). This Mn drop suggests desorption/dissolution from SPM possibly associated to intense physical–chemical (i.e. redox, pH) and/or microbiological changes along the rapidly increasing ionic strength gradient. Mn desorption from SPM is supported by a consistent dissolved Mn peak detected at the beginning of TMZ ($19\ \mu g\ L^{-1}$) which is more than an order of magnitude higher than concentrations detected either in freshwater ($0.8–1.6\ \mu g\ L^{-1}$) or the marine sector ($< 0.3–3.3\ \mu g\ L^{-1}$; Fig. 6). Mn remobilization from SPM associated to dissolved peaks has been previously observed during freshwater-marine mixing and tentatively attributed to pH shifts (L'Her Roux et al., 1998) or microorganism activity releasing Mn^{+2} from oxides in Mn-enriched organic aggregates (Klinkhammer and McManus, 2001). A similar particulated Mn reduction coincident with dissolved maxima has been also observed in the Saint Lawrence River-Estuary and attributed to both, dissolution from SPM and resuspension of bottom sediments impoverished in Mn (Yeats, 1990). However, in our study bottom sediments are enriched in Mn relative to SPM in the TMZ (i.e. resuspension would not "dilute" SPM concentrations). Moreover, the other metals do no show such a decrease in SPM as Mn in the turbidity maximum, as would be expected if resuspension is the driving cause. Bottom sediments from the TMZ effectively present a surficial Mn enrichment (Fig. 6) suggesting also the presence of an internal source. This reflects the well known mobility of Mn in anoxic sediments, i.e. redox mediated dissolved Mn^{+2} evasion from solid oxides in anoxic layers with partial reprecipitation at the oxic sediment surface (Sundby et al., 1981; Yeats, 1990; Laslett and Balls, 1995).

4. Conclusions

The strong environmental gradients which characterize the Samborombón Bay (salinity: 0.11–31.4; turbidity: 21 to $> 999\ mg\ L^{-1}$ peaking at the TMZ) exert a marked control on sediment deposition and trace metal dynamics. SPM trace metal concentrations showed two general patterns: homogeneous spatial distributions (Fe, Zn) and progressive enrichment from the TMZ to the maritime area (Cu, Ni) reflecting the shift from abundant detrital to scarce, more organic material along the land–sea gradient. The influence of the TMZ is clearly reflected in bottom sediments by the enrichment of flocculated clays which in turns control the distribution of TOC and trace metals resulting in a prevailing decreasing land–sea gradient. Most sediment samples are below sediment quality guidelines for trace metals with no offshore gradients indicating a good ecotoxicological condition and the virtual absence of coastal pollution sources.

Mn has a particular behavior along the salinity gradient denoting intense dissolved–particulated phase changes both in the water column and bottom sediments. An average 36% drop of particulate Mn concentrations observed in parallel with a strong dissolved peak suggests rapid desorption/dissolution at the beginning of the ionic gradient. Concomitant with the SPM minima, bottom sediments display an average 72% Mn enrichment in the TMZ relative to the riverine sector reflecting the diffusive escape from anoxic sediments and reprecipitation in oxic surface layers. More detailed studies are needed to better elucidate the relative importance of these factors controlling the behavior, internal trapping and final transport of Mn to the sea.

Acknowledgements

Financial support was partially provided by the Argentinean National Research Council (CONICET) and the Research Commission from Buenos Aires State (CIC).

References

Acha, E.M., Mianzan, H., Guerrero, R., Carreto, J., Giberto, D., Montoya, N., Carignan, M., 2008. An overview of physical and ecological processes in the Río de la Plata Estuary. Cont. Shelf Res. 28, 1579–1588.
Biggs, R.B., Howell, B.A., 1984. The estuary as a sediment trap: alternate approaches to estimating its filtering efficiency. In: Kennedy, V.S. (Ed.), The Estuary as a Filter. Academic Press, Orlando, pp. 107–129.
Carol, E.S., Braga, F., Kruse, E.E., Tosi, L., 2014. A retrospective assessment of the hydrological conditions of the Samborombón coastland (Argentina). Ecol. Eng. 67, 223–237.
Carreto, J.I., Montoya, N., Akselman, R., Carignan, M.O., Silva, R.I., Cucchi Colleoni, D.A., 2008. Algal pigment patterns and phytoplankton assemblages in different water masses of the Río de la Plata maritime front. Cont. Shelf Res. 28, 1589–1606.
CCME, 2001. Canadian sediment quality guidelines for the protection of aquatic life: summary tables, Canadian Environmental Quality Guidelines. Canadian Council of Ministers of the Environments, Winnipeg, p. 1999.
Colombo, J.C., Cappelletti, N., Barreda, A., Migoya, M.C., Skorupka, C.N., 2005a. Vertical fluxes and accumulation of PCBs in coastal sediments of the Río de la Plata estuary, Argentina. Chemosphere 61, 1345–1357.
Colombo, J.C., Cappelletti, N., Lasci, J., Migoya, M.C., Speranza, E., Skorupka, C.N., 2005b. Sources, vertical fluxes and accumulation of aliphatic hydrocarbons in coastal sediments of the Río de la Plata Estuary, Argentina. Environ. Sci. Technol. 39, 8227–8234.
Colombo, J.C., Cappelletti, N., Lasci, J., Migoya, M.C., Speranza, E., Skorupka, C.N., 2006. Sources, vertical fluxes and equivalent toxicity of aromatic hydrocarbons in coastal sediments of the Río de la Plata Estuary, Argentina. Environ. Sci. Technol. 40, 734–740.
Depetris, P.J., Probst, J., Pasquini, A.I., Gaiero, D.M., 2003. The geochemical characteristics of the Paraná River suspended sediment load: an initial assessment. Hydrol. Process. 17, 1267–1277.
Drago, E.C., Amsler, M.L., 1988. Suspended sediment at a cross section of the Middle Paraná River: concentration, granulometry and influence of the main tributaries. Proc. Porto Alegre Symp., 381–396 (IAHS Publ. no. 174).
Drago, E.C., Amsler, M.L., 1998. Bed sediment characteristics in the Paraná and Paraguay Rivers. Water Int. 23, 174–183.
Folk, R.L., 1980. Petrology of Sedimentary Rocks, Hemphill Publishing Company, Austin, TX.
Framiñan, M.B., Brown, O.B., 1996. Study of the Río de la Plata turbidity front, Part I: spatial and temporal distribution. Cont. Shelf Res. 16, 1259–1282.
Framiñan, M.B., Etala, M.P., Acha, E.M., Guerrero, R.A., Lasta, C.A., Brown, O.B., 1999. Physical characteristics and processes of the Río de la Plata Estuary. In: Perillo, G.M.E., Piccolo, M.C., Pino-Quivira, M. (Eds.), Estuaries of South America, Their Geomorphology and Dynamics. Springer, Berlin, pp. 161–194.
Guerrero, R.A., Acha, E.M., Framiñan, M.B., Lasta, C.A., 1997. Physical oceanography of the Río de la Plata Estuary, Argentina. Cont. Shelf Res. 17, 727–742.
Hedges, J.I., Keil, R.G., Benner, R., 1997. What happens to terrestrial organic matter in the ocean? Org. Geochem. 27, 195–212.
Hseu, Z.Y., Chen, Z.S., Tsui, C.C., Tsai, C.C., Tsaui, C.C., Cheng, S.F., Liu, C.L., Lin, H.T., 2002. Digestion methods for total heavy metals in sediments and soils. Water Air Soil Pollut. 141, 189–205.
Hughes, M.G., Harris, P.T., Hubble, T.C.T., 1998. Dynamics of the turbidity maximum zone in a micro-tidal estuary: Hawkesbury River, Australia. Sedimentology 45, 397–410.
Klinkhammer, G.P., McManus, J., 2001. Dissolved manganese in the Columbia River estuary: production in the water column. Geochim. Cosmochim. Acta 65, 2835–2841.

Laslett, R.E., Balls, P.W., 1995. The behaviour of dissolved Mn, Ni and Zn in the Forth, an industrialised, partially mixed estuary. Mar. Chem. 48, 311–328.
Lasta, C.A., 1995. La Bahía Samborombón: zona de desove y cría de peces. National University of La Plata, Argentina (Ph.D. thesis).
L'Her Roux, L., Le Roux, S., Appriou, P., 1998. Behaviour and speciation of metallic species Cu, Cd, Mn and Fe during estuarine mixing. Mar. Pollut. Bull. 36, 56–64.
Mianzan, H., Lasta, C., Acha, E., Guerrero, R., Macchi, G., Bremec, C., 2001. The Río de la Plata Estuary, Argentina-Uruguay. In: Seeliger, U., Kjerfve, B. (Eds.), Ecological Studies. Springer-Verlag, Berlin, pp. 185–204.
Moreira, D., Simionato, C.G., Gohin, F., Cayocca, F., Tejedor, M., Luz Clara, 2013. Suspended matter mean distribution and seasonal cycle in the Río de La Plata estuary and the adjacent shelf from ocean color satellite (MODIS) and in-situ observations. Cont. Shelf Res. 68, 51–66.
Morris, A.W., Loring, D.H., Bale, A.J., Howland, R.J.M., Mantoura, R.F.C., Woodward, E. M.S., 1982. Particle dynamics, particulate carbon and the oxygen minimum in an estuary. Oceanol. Acta 5, 349–353.
Piedra-Cueva, I., Fossati, M., 2007. Residual currents and corridor of flow in the Río de la Plata. Appl. Math. Model. 31, 564–577.
Stecko, J.R.P., Bendell-Young, L.I., 2000. Contrasting the geochemistry of suspended particulate matter and deposited sediments within an estuary. Appl. Geochem. 15, 753–775.
Sundby, B., Silverberg, N., Chesselet, R., 1981. Pathways of manganese in an open estuarine system. Geochim. Cosmochim. Acta 45, 293–307.
Tatone, L.M., Bilos, C., Skorupka, C., Colombo, J.C., 2009. Vertical Fluxes and Accumulation of Trace Metals in Superficial Sediments of the Río de la Plata Estuary, Argentina. Bull. Environ. Contam. Toxicol. 83, 913–919.
Tatone, L.M., Bilos, C., Skorupka, C., Colombo, J.C., 2013. Trace metals in settling particles from the sewage impacted Buenos Aires Coastal area in the Río de la Plata Estuary, Argentina. Bull. Environ. Contam. Toxicol. 90, 318–322.
Woodruff, J.D., Geyer, W.R., Sommerfield, C.K., Driscoll, N.W., 2001. Seasonal variation of sediment deposition in the Hudson River estuary. Mar. Geol. 179, 105–119.
Wu, J., Liu, J.T., Wang, X., 2012. Sediment trapping of turbidity maxima in the Changjiang Estuary. Mar. Geol. 303–306, 14–25.
Yeats, P.A., 1990. Reactivity and transport of nutrients and metals in the St. Lawrence Estuary. In: El-Sabh, M.I., Silverberg, N. (Eds.), Oceanography of a Large-Scale Estuarine System: The St. Lawrence. Springer-Verlag, New York, pp. 155–169.
Zhang, W., Feng, H., Chang, J., Qu, J., Xie, H., Yu, L., 2009. Heavy metal contamination in surface sediments of Yangtze River intertidal zone: an assessment from different indexes. Environ. Pollut. 157, 1533–1543.